EES Catalysis

COMMUNICATION

View Article Online
View Journal | View Issue

Cite this: *EES Catal.*, 2023, 1, 117

Received 15th October 2022,
Accepted 28th November 2022

DOI: 10.1039/d2ey00071g

rsc.li/eescatalysis

Revealing the activity and selectivity of ppm level copper in gas diffusion electrodes towards CO and CO_2 electroreduction†

Xiang Lyu, [ab] Jianlin Li, [b] Tianyu Zhang,[a] Zhengyuan Li,[a] In-hui Hwang,[c] Chengjun Sun,[c] Charl J. Jafta, [b] Jun Yang,[b] Todd J. Toops,[d] David A. Cullen, [e] Alexey Serov*[b] and Jingjie Wu *[a]

Cu is a unique metal that catalyzes carbon monoxide/carbon dioxide (CO/CO_2) to form high-order hydrocarbons and oxygenates through the CO/CO_2 reduction reaction (CO/CO_2RR) at decent selectivity and productivity. While this has been shown, the limits of the system are still unknown, *i.e.*, the minimum amount of Cu needed for the CO/CO_2RR, and the maximum activity that trace amounts of Cu can achieve. Here, we have investigated the activity and selectivity of trace Cu with atomic dispersion over a range of loadings below 2 μg cm^{-2} and have quantified the mass activity/turnover frequency (TOF) of trace Cu catalysts. A Cu loading of at least 0.042 μg cm^{-2} initiates the CORR activity with 30% faradaic efficiency (FE) at a partial current density of 102 mA cm^{-2} forming predominantly CH_4. The selectivity moves to C_2-based products (CH_3COO^-, C_2H_4, and CH_3CH_2OH) with 70% FE as the Cu loading increases to 0.333 μg cm^{-2}, and increasing the Cu loading to 0.812 μg cm^{-2} results in a 78% FE to C_2 with CH_3COO^- accounting for 42% of this. The highest mass activity for CH_4 reaches 2435 A mg^{-1} of Cu, corresponding to a TOF of 267 s^{-1}, while C_2 activity reaches 584 A mg^{-1} of Cu, leading to a TOF of 145 s^{-1}. Both TOFs are several orders of magnitude higher than the reported values. Different from the CORR, the CO_2RR demands a higher Cu loading and primarily generates C_1 (*e.g.*, CO and CH_4). Metal impurities can be extended to others that are active towards the CO_2RR, such as Zn for CO_2-to-CO conversion. Thus, we suggest that the effect of trace metal impurities must be quantified when developing carbon-based metal-free and coordinated single-atom catalysts for the CO/CO_2RR in order to avoid overestimating their activity.

Broader context

Carbon dioxide (CO_2) removal and utilization have become an essential feature of climate mitigation. The electrochemical CO_2 reduction reaction (CO_2RR) to form valuable chemicals and fuels utilizing renewable energy is a promising strategy contributing to the carbon-net-zero goal. A catalyst with high activity and selectivity is critical to enabling the large-scale application of the CO_2RR. Cu-based catalysts are uniquely known hydrocarbon- and oxygenate-selective metal catalysts. Meanwhile, metal-free carbon-based and metal–nitrogen–carbon (M–N–C with metals of Fe, Ni, and Co) single-atom catalysts have been developed as alternatives to conventional metal catalysts for the CO/CO_2 reduction reaction (CO/CO_2RR). Since trace Cu on carbon-based supports was reported to show activity towards the CO_2RR, the performance overestimation of metal-free and M–N–C catalysts during the CO/CO_2RR is a concern. Currently, two questions remain elusive: what is the lowest limit Cu loading to show activity for the CO/CO_2RR, and how high is the activity that trace amounts of Cu can achieve? Both questions are critical to scientifically evaluate the intrinsic performance of the catalysts during the CO/CO_2RR. In this work, we answered both questions by revealing the activity and selectivity of ppm level copper in gas diffusion electrodes towards the CO/CO_2RR.

Introduction

The electrochemical CO_2 reduction reaction (CO_2RR) to form valuable chemicals and fuels utilizing renewable energy has attracted remarkable attention, as it is beneficial in producing value-added products while simultaneously consuming CO_2 under mild operating conditions.[1–4] Nevertheless, the practical cost is still high for large-scale applications partly because of the low selectivity, efficiency, and durability of existing electrocatalysts.[5–7] The state-of-the-art electrocatalysts for the CO_2RR are metallic.[8–11] Ag, Au, and Zn mainly convert CO_2 to carbon monoxide (CO),[12–15] while Sn and Bi are selective to formate ($HCOO^-$) *via* a two-electron reduction process in the CO_2RR.[16–18] Cu stands out as the only known metal catalyst capable of generating high-order products such as C_1–C_2 hydrocarbons (*e.g.*, CH_4 and C_2H_4) and C_2^+ oxygenates (*e.g.*, CH_3CH_2OH, CH_3COOH, and

[a] *Department of Chemical and Environmental Engineering, University of Cincinnati, Cincinnati, OH, USA. E-mail: jingjie.wu@uc.edu*
[b] *Electrification and Energy Infrastructures Division, Oak Ridge National Laboratory, Oak Ridge, TN 37831, USA. E-mail: serova@ornl.gov*
[c] *X-Ray Science Division, Argonne National Laboratory, IL 60439, USA*
[d] *Buildings and Transportation Science Division, Oak Ridge National Laboratory, Oak Ridge, TN 37831, USA*
[e] *Center for Nanophase Materials Sciences, Oak Ridge National Laboratory, Oak Ridge, Tennessee, 37831, USA*

† Electronic supplementary information (ESI) available. See DOI: https://doi.org/10.1039/d2ey00071g

C_3H_7OH,) beyond the $2e^-$ reduction route.[19–23] Moreover, Cu is also the unique metal that catalyzes the electrochemical CO reduction reaction (CORR), a critical intermediate reaction in the CO_2RR, to form a similar distribution of C_{2+} hydrocarbons and oxgenates.[24,25]

A trace level of Cu nanoparticles (*e.g.*, 119 ppm) in graphene oxide loaded on a glass carbon substrate exhibited electrochemical activity towards the CO_2RR in an H-cell.[26] The carbon products were only C_1 (CO, CH_4, and HCOOH) with a total faradaic efficiency (FE) of about 15% and a total current density of around 5 mA cm^{-2} at −1.3 V *versus* reversible hydrogen electrode (*vs.* RHE throughout the text). Fu *et al.* prepared atomically dispersed Cu atoms with a low loading of 69 μg cm^{-2} on nitrogen-rich porous carbon supports and then loaded them onto a carbon paper substrate as gas diffusion electrodes (GDEs).[27] They reported ~60% FE to C_2^+ products in the CORR under a total current density of 75 mA cm^{-2} at −0.7 V, while CH_4 formation was negligible. Rong *et al.* synthesized atomically dispersed Cu atoms on a graphdiyne support loaded on a carbon paper substrate to make GDEs as well.[28] They observed that the major product of the CORR switched from C_1/CH_4 (57.3% FE) to C_2 (80% FE) at −1 V as the atomically dispersed Cu loading increased from 7.5 to 226 μg cm^{-2}. Those findings indicated that the content of trace Cu on carbon-based supports can substantially influence the electrochemical activity and selectivity in the CO/CO_2RR. However, the maximum mass activity and turnover frequency (TOF) in the CO/CO_2RR that can be achieved with trace Cu is still unknown. Moreover, understanding how decreasing the Cu loading impacts selectivity in the CO/CO_2RR is also unknown.

An alternative approach under investigation is the use of metal-free carbon catalysts and metal–nitrogen–carbon (M–N–C with metals of Fe, Ni, and Co). Most carbon and M–N–C catalysts show predominant products of C_1 (*e.g.*, CO and CH_4) in the CO/CO_2RR.[29–33] For example, the graphitic-N doped graphene-like carbon catalyst was reported to convert CO_2 to CO with a 95% FE and partial current density of 9.07 mA cm^{-2} at −0.72 V.[31] N-doped graphene quantum dots (NGQDs) with functionalized electron-donating groups (*e.g.*, –OH and $–NH_2$) could catalyze CO_2 to CH_4 with both high selectivity (70% FE) and production rate (partial current density of 200 mA cm^{-2}) at −0.85 V.[32] The single Zn atom supported on a microporous N-doped carbon catalyst was reported to catalyze CO_2 to CH_4 with an 85% FE and partial current density of 31.8 mA cm^{-2} at −1.8 V (*vs.* Hg/$HgCl_2$).[34] A few carbon catalysts were also reported to form C_2 products.[35–37] Rigorous evaluation of the activity to the CO/CO_2RR of metal-free catalysts should consider the potential effect of trace metal impurities like Cu and Zn because metal impurities will be introduced from reactants/precursors during synthesis of the catalyst and from electrolytes during electrolysis.[26,38–43] Therefore, a systematic evaluation of trace metal loading-dependency on GDE was performed as it relates to the CO/CO_2RR activity and selectivity.

Herein, to clearly reveal the effect of low levels (ppm) of Cu on the CO/CO_2RR performance, trace amounts of Cu with a range of loadings was directly loaded onto carbon paper (CP, Sigracet 39BB gas diffusion layer) *via* a facile impregnation method. This loading method does not use any additional carbon supports as reported in the literature and subsequently eliminates the effect of the carbon support on the performance. A significant activity towards the CORR is observed on trace Cu-loaded GDE when the loading is higher than 0.042 μg cm^{-2} (4.9 ppm referred to the electrode mass). Cu loading down to 0.042 μg cm^{-2} can lead to up to 50% FE of carbon products, with CH_4 as the major carbon product, at −0.76 V in the CORR. The primary product switches from C_1 to C_2 with a total 70% FE at −0.74 V when the Cu loading increases from 0.042 to 0.333 μg cm^{-2}. The CO_2RR requires a higher Cu content than the CORR to trigger the activity. Only predominant products of C_1 are observed at a Cu loading of 0.812 μg cm^{-2}. The primary product switches from CO to CH_4 with the increase in overpotential. These findings indicate that a ppm level of Cu in the electrodes has a significant impact on the CO/CO_2RR, especially on the CORR. In addition, this study proposes the importance of the design of Cu catalysts at the atomic scale to maximize the specific activity towards the CO/CO_2RR.

Results and discussion

CORR activity over a trace Cu-loaded carbon paper.

The electrocatalytic activity and selectivity towards CO/CO_2 reduction were evaluated in a custom flow cell. The geometric area of the CP electrode is 2.8 cm^2 (1.67 cm × 1.67 cm), of which 1.0 cm^2 (1.0 cm × 1.0 cm) is the active area matching the dimensions of the flow field and the cathode compartment (more details in the Experimental methods of the ESI†). The CP electrodes containing a Cu loading of 0.812 μg cm^{-2} (denoted as CP–$Cu_{0.812}$) were first investigated for the CORR. CP–$Cu_{0.812}$ electrodes exhibit outstanding electrochemical activity to the CORR with the highest FE of carbon products reaching 83% at −0.64 V (Fig. 1a). The FE of C_2 (including CH_3COO^-, C_2H_4, and CH_3CH_2OH) products maintains high (>48%) in a wide potential window from −0.6 to −0.87 V (Fig. 1b), and the highest 78% FE of C_2 products is achieved at −0.64 V (Fig. 1b). In contrast, the FE of CH_4 only rises to a maximum of 19.1% as the potential is negatively swept to −0.86 V. The partial current densities for both C_2 and CH_4 (j_{C_2} and j_{CH_4}) monotonically increase as the potential is swept cathodically. The j_{C_2} and j_{CH_4} climb to 429 and 170 mA cm^{-2}, respectively, at −0.86 V (Fig. 1c). The total current density of the carbon products with a Cu loading of 0.812 μg cm^{-2} reaches 599 mA cm^{-2} at −0.86 V, which is even higher than the Cu nanocube[44] and nanosheet[45] catalysts with loadings as high as 500 μg cm^{-2} under similar operating conditions, indicating that the trace Cu on CP exhibits extraordinary electrochemical activity toward the CORR.

To systematically investigate the impact of trace Cu loadings on the CORR, we prepared CP electrodes with Cu loadings ranging from 0.016 to 1.53 μg cm^{-2}, as shown in Table S1 (ESI†). Notably, the Cu loading in the as-received pristine CP is 0.016 μg cm^{-2} (PCP–$Cu_{0.016}$), and thus, the total Cu content in the prepared CP electrodes includes this Cu impurity in the PCP. The CORR performance of the CP electrodes with different

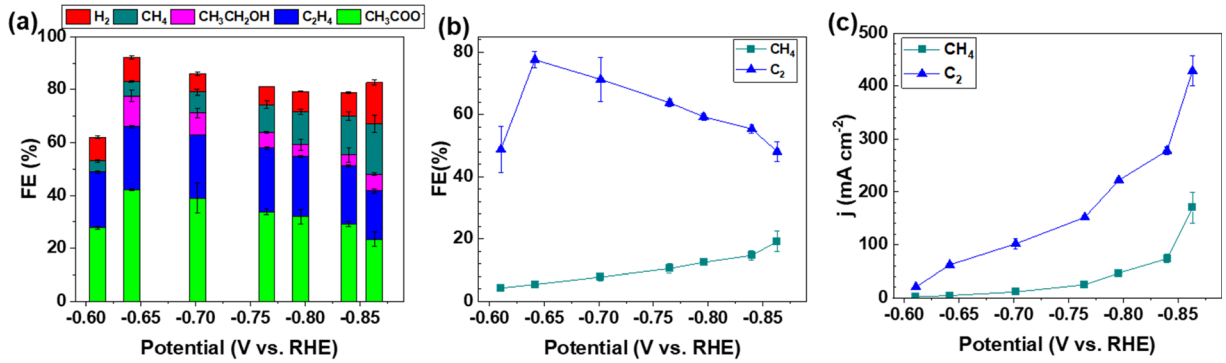

Fig. 1 (a) Product distribution during the CORR as a function of the applied potential on the CP–$Cu_{0.812}$ electrode. (b) FEs of C_2 and CH_4. (c) The partial current density of C_2 and CH_4. The error bars represent the standard deviation from the measurements of three independent electrodes.

Cu contents is shown in Fig. 2 and Fig. S2 (ESI†). A significant effect on the CORR is observed when the Cu loading exceeds 0.042 μg cm^{-2} Cu (4.9 ppm Cu in the total electrode), and 50% FE of carbon products with the predominant carbon product of CH_4 is obtained at this Cu level. The peak FE of 39% for CH_4 is reached with CP–$Cu_{0.070}$ electrodes. The primary product switches to C_2 when the Cu loading further increases to 0.333 μg cm^{-2}, indicating that the C–C coupling reaction is accelerated with the existence of more Cu active sites. The highest C_2 FE of 78% is achieved at −0.64 V with a Cu loading of 0.812 μg cm^{-2}. The current density of C_2 exhibits a positive correlation with the Cu loading, while the current density of CH_4 remains in a similar range with other Cu loadings.

The mass activity for C_2 reaches 584 A mg^{-1} of Cu with a FE of 57% at −0.86 V for the CP–$Cu_{0.333}$ electrodes, which is 2–5

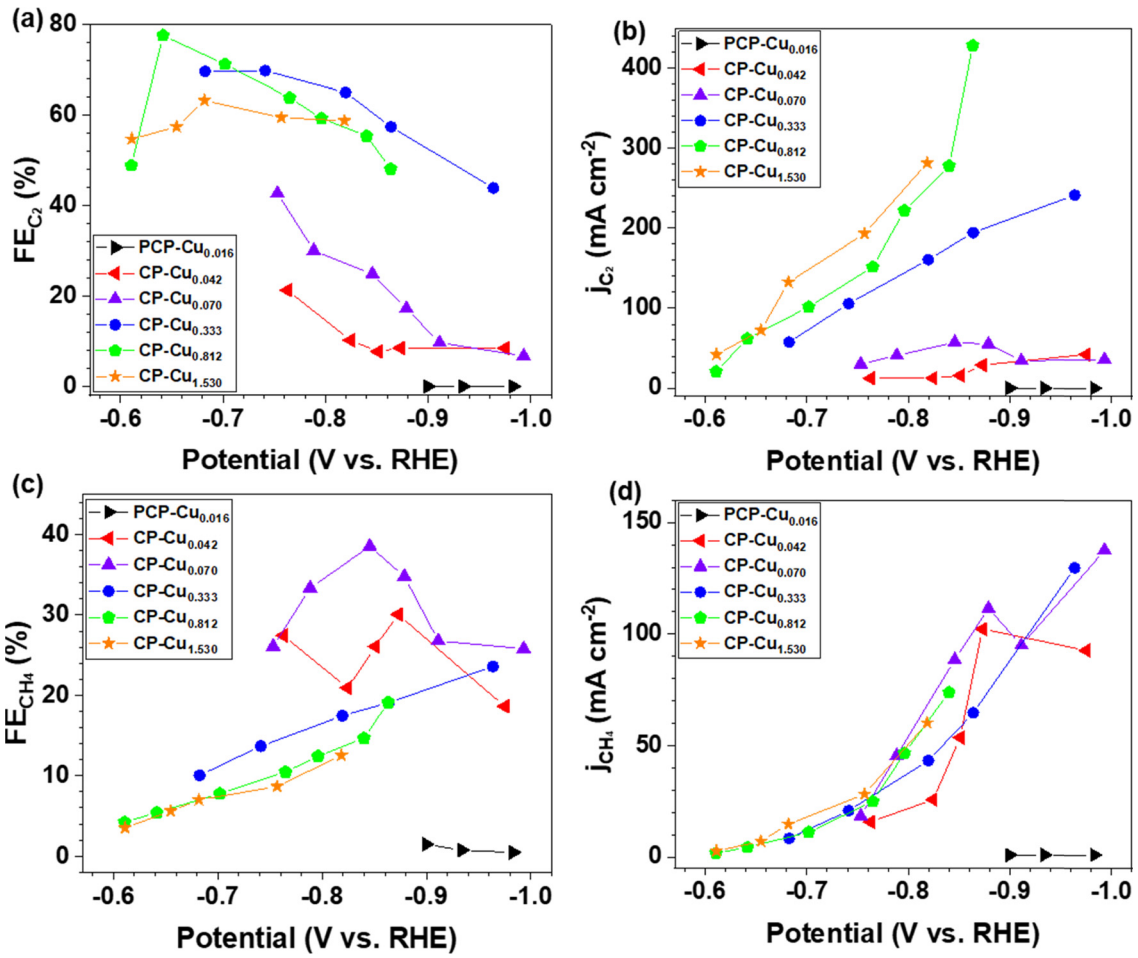

Fig. 2 (a) The partial current density and (b) FE of C_2 during the CORR as a function of the applied potential using CP–Cu electrodes with various Cu loadings. (c) The partial current density and (d) FE of CH_4 as a function of the applied potential using CP–Cu electrodes with various Cu loadings.

orders of magnitude higher than those reported in the literature (Table S2, ESI†). The mass activity for CH_4 rises to 2435 A mg^{-1} of Cu with a FE of 30.1% at −0.87 V using the CP–$Cu_{0.042}$ electrodes, which is an increase of 4 orders of magnitude compared with similar Cu/C electrode reported values.[12] This is a clear indication that a trace level of Cu can be very active and should always be accounted for in the CORR experiments.

A control experiment was carried out to evaluate the effect of the CP treatment with the solvent mixture of DI water and IPA but without additional $CuCl_2$ on the CORR. After exposure to the solution, the Cu loading declines from 0.016 to 0.006 μg cm^{-2}, indicating the Cu contamination in the PCP can be partially dissolved in the solvent mixture. The electrochemical results of the CP–$Cu_{0.006}$ electrodes are shown in Fig. S3 (ESI†). Only trace CH_4 is produced and H_2 predominates, which is a similar performance to PCP–$Cu_{0.016}$. Another control experiment was performed to investigate the effect of solvent on the Cu impregnation, where the highest concentration of 5 mM of $CuCl_2$ in DI water was used. The performance of this control electrode for the CORR is displayed in Fig. S4 (ESI†). The HER exclusively occurs under current densities from 107 to 321 mA cm^{-2}, and only trace amounts of CH_4 with a FE < 2.2% are detected. This finding suggests that the Cu ions in pure DI water could not be loaded onto the CP substrate, as the CP surface is highly hydrophobic. Fig. S5 (ESI†) shows contact angle measurements on CP with pure DI water and a mixture of DI water/IPA (v/v: 1/1). The contact angle decreases from 169 to 42 °C when replacing the pure DI water with the solvent mixture.

The product distribution of the CORR as a function of the trace Cu loading is further plotted in Fig. 3. The FEs of each CORR product under different Cu loadings are compared at the current density of around 130 mA cm^{-2} (Fig. 3a). The peak FE of 33% for CH_4 is achieved with 0.070 μg cm^{-2} Cu loading. The CH_3COO^- is predominant with a peak FE of 41% at a Cu loading of 0.333 μg cm^{-2}. The results indicate that the trace level of Cu is already very active towards the CORR to form CH_3COO^-. The FE ratio of C_1/C_2 is 1.1 with the CP–$Cu_{0.070}$ electrode, and it drops to 0.11 with the CP–$Cu_{0.812}$ electrode, indicating the selectivity varies by 10 times after 0.742 μg cm^{-2} Cu is added. Fig. 3b depicts the product distribution of the CORR at around 330 mA cm^{-2} as the trace Cu loading increases, and a similar trend is observed with 130 mA cm^{-2}. The notable difference is that the FE of C_2 decreases while the FE of C_1 increases slightly at a higher current density and overpotential, as the high overpotential prefers CH_4 formation.[46–48]

The performance of CO_2RR with different Cu loadings in carbon paper

The electrochemical activity of trace Cu on CP was also evaluated for the CO_2RR (Fig. S6, ESI†). The low (CP–$Cu_{0.070}$) and high (CP–$Cu_{0.812}$) Cu loading electrodes were chosen for the CO_2RR since these electrodes exhibit the predominant selectivity towards C_1 and C_2 in the CORR, respectively. The highest FE of carbon products with the CP–$Cu_{0.070}$ electrode in the CO_2RR is 62%, lower than in the CORR (83%), indicating that the CO_2RR is less sensitive to trace Cu than the CORR. It is worth pointing out that trace Cu favors formation of C_1 products in the CO_2RR, which is different from C_2 products being favored in the CORR. The predominant product is CO at low potentials, and it transitions to CH_4 when the potential is swept more negatively for both CP–$Cu_{0.070}$ and CP–$Cu_{0.812}$ electrodes. The peak FE of CO is 26% appearing at −0.57 V for the CP–$Cu_{0.070}$ electrode while the maximum FE of CH_4 is 24% at −0.67 V. The CP–$Cu_{0.812}$ electrode shows the highest FE of CO, 43%, at −0.55 V and 38% FE of CH_4 is achieved at −0.83 V. The CP–$Cu_{0.070}$ electrodes possess mass activities of 155 and 375 A mg^{-1} Cu for CO and CH_4, respectively, which are 2–3 orders of magnitude higher than those reported in the literature (Table S2, ESI†). This finding indicates that Cu impurities as low as 0.070 μg cm^{-2} (8.2 ppm relative to the total electrode) can significantly affect the performance of carbon catalysts for C_1 (*e.g.*, CO and CH_4) generation. Our previous work found that functionalized N-doped graphene quantum dots (NGQDs) could catalyze CO_2 to CH_4 with a high selectivity of

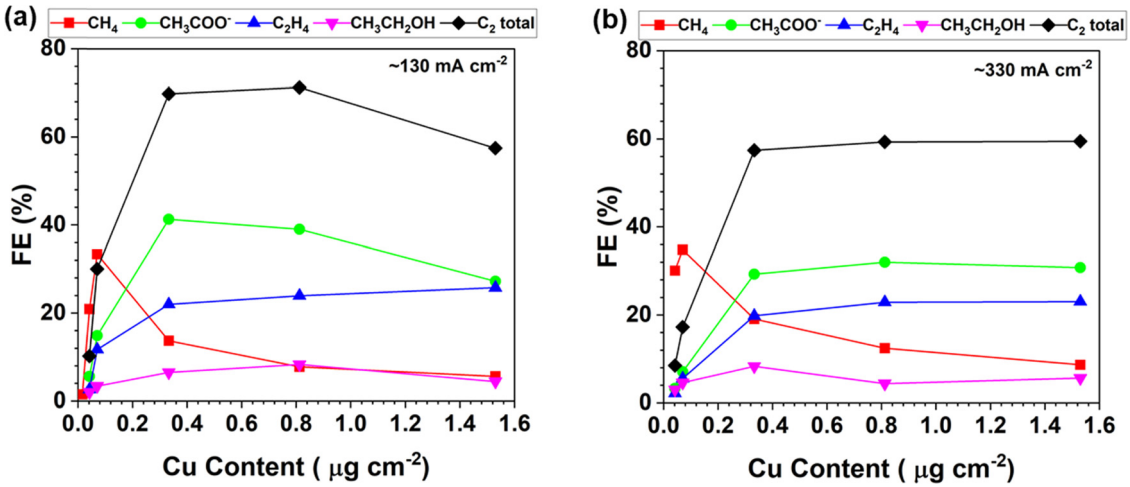

Fig. 3 Product distribution of the CORR as a function of the Cu loading in the electrodes at the current density of around 130 mA cm^{-2} (a) and 330 mA cm^{-2} (b).

70% FE at −0.85 V, and the Cu impurity on electrodes is 0.056 μg cm^{-2}.[32] We observed that the highest FE of CH_4 is 24% at −0.67 V for 0.070 μg cm^{-2} Cu and 14% at −0.81 V for 0.042 μg cm^{-2} Cu (Fig. S6, ESI†). Compared to trace Cu only, the functionalized NGQDs requires a more negative potential to reach the maximum FE of C_2H_4. The facts indicate that both functionalized NGQDs and trace Cu may contribute to CH_4 formation in the CO_2RR, even though functionalized NGQDs play a more significant role.

The trace metal effect on the CO/CO_2RR can be extended to other metal impurities, such as Ag, Au, Zn, Sn, and Bi. To verify this hypothesis, we loaded trace Zn (∼1.6 μg cm^{-2}) onto the CP by impregnating CP in a 5 mM $ZnCl_2$ solution (2 mL, $H_2O_{(v)}$/$IPA_{(v)}$ = 1/1 solvent) for 1 h. The electrochemical activity of trace Zn to the CO_2RR is shown in Fig. S7 (ESI†). The FE of CO is higher than 60% in the wide testing potential range of −0.65 to −1.08 V, and the total current density reaches 300 mA cm^{-2} at −1.08 V, indicating that the trace Zn on the CP exhibits outstanding activity for CO generation. M–N–C catalysts are commonly employed as single-atom metal electrocatalysts for catalyzing CO_2 to CO with high FEs.[41–43] However, to the best of our knowledge, the metal impurities, such as Au, Ag, and Zn, were never determined and evaluated with those M–N–C catalysts, which may result in the overestimation of M–N–C catalyst performance.

Chemical structure of Cu

In order to correlate the chemical structure and oxidation status of Cu with the electrochemical activity towards the CORR/CO_2RR, the trace Cu structure was characterized by a combination of electron microscopy and spectroscopy. The microstructure of the CP–$Cu_{0.812}$ post-electrode was characterized by scanning electron microscopy (SEM), as shown in Fig. S8 (ESI†). No aggregate of Cu at the micron size was observed. The corresponding energy dispersive X-ray spectroscopy (EDS) elemental mapping is shown in Fig. S9 (ESI†). It is well known that characterization of ppm level Cu in carbon materials is a challenge. The Cu structure on the CP–$Cu_{0.812}$ post-electrode was determined further with aberration-corrected scanning transmission electron microscope (AC-STEM). No metal nanoparticles or clusters were found, and only a few Cu single atoms were observed after many attempts, as shown in Fig. 4a and b.

Fig. 4c and d show the high-resolution X-ray photoelectron spectroscopy (XPS) spectra of Cu 2p of pre- and post-electrodes, respectively. No notable peaks of Cu 2p are visible on any electrodes due to the ultralow Cu loading. X-ray absorption spectroscopy (XAS) was employed to further investigate the chemical structure of Cu species at the atomic scale. Fig. 4e presents the X-ray absorption near edge structure (XANES) spectra of the Cu K-edge for CP–$Cu_{0.070}$ (pre- and post-), CP–$Cu_{0.333}$ (post-), and CP–$Cu_{0.812}$ (pre- and post-) electrodes. The Cu shows a higher energy absorption edge at higher Cu loadings, suggesting an increase of Cu valence with an increase of Cu loading. The possible reason is that the high-loading Cu species are more susceptible to being oxidized by oxygen in the air due to the impregnation method. Compared to the pre-electrodes of CP–$Cu_{0.812}$, the post-electrode shows lower Cu energy due to the reduction of Cu in the CORR. The energy absorption from all electrodes is in the range between CuO and Cu_2O, indicating that Cu in the post-reaction electrodes has a chemical state of $Cu^{\delta+}$ ($1 < \delta < 2$). Fig. 4f displays the Cu Fourier-transformed k^3-weighted extended X-ray absorption fine structure (EXAFS) in R space. Only a notable peak at *ca.* 1.5 Å, which is associated with Cu–C/O scattering, is observed in both the pre-and post-electrodes of CP–$Cu_{0.812}$.[28,49,50] No Cu–Cu bonding peak is seen for any electrodes, which confirms that the Cu species are atomically dispersed on CP. According to the analysis above, we conclude that the high electrochemical activity towards the CO/CO_2RR comes from a trace level of atomically dispersed Cu with a chemical state of $Cu^{\delta+}$ ($1 < \delta < 2$).

Since the Cu species are atomically dispersed in the CP, the TOF of trace amounts of Cu catalysts for the CO/CO_2RR were calculated assuming the existence of single atom Cu. For the CP–$Cu_{0.333}$ electrodes, the TOF for the CO-to-C_2 products conversion reaches 145 s^{-1} at −0.86 V, which is 4 orders of magnitude higher than those reported in the literature (Table S3, ESI†). For the CP–$Cu_{0.042}$ electrodes, the TOF for the CO-to-CH_4 conversion achieves 267 s^{-1} at −0.87 V, which has increased by 2 orders of magnitude compared with reported values in the literature (Table S3, ESI†).

Proposed mechanism for the CO/CO_2RR in the trace Cu loaded CPs

We attempted to propose the reaction mechanism of the CO/CO_2RR on trace Cu loaded CPs based on documented theoretical investigations and our experimental observations. At a very low Cu loading in the CP (<0.333 μg cm^{-2}), the primary product in the CORR is CH_4, while it switches to C_2 when the Cu loading is higher than 0.333 μg cm^{-2}. The predominant product switches from C_1 to C_2 with an increased Cu loading in the CP, while the Cu species remain atomically dispersed in the CP. The density of the Cu single atom is hypothesized to be responsible for the switch of the predominant product in the CORR. A low density of Cu loading prefers the C_1 products, while a high density of Cu loading favors the C_2 products. It was reported that the single-site Cu can facilitate the protonation of CO* to CHO* and then form C_1 products due to the strong chemisorption of H* and the high partial pressure of CO in the CORR.[28] The lack of Cu pair active sites makes C_1 the primary product. The C–C coupling is accelerated with the increase of atomic Cu density.[27] The C–C coupling reaction can proceed *via* either the Eley–Rideal mechanism or the Langmuir–Hinshelwood mechanism. The Eley–Rideal mechanism is supposed to be predominant in the CORR due to the high partial pressure of CO.

Distinguished from the CORR, the main product is only C_1 (*e.g.*, CO and CH_4) in the CO_2RR with trace amounts of Cu, indicating that the C–C coupling in the CO_2RR is more challenging than that in the CORR. One possible reason is that it is difficult for the C–C coupling to occur by the Eley–Rideal mechanism due to the low pressure of CO under the CO_2RR conditions. The other

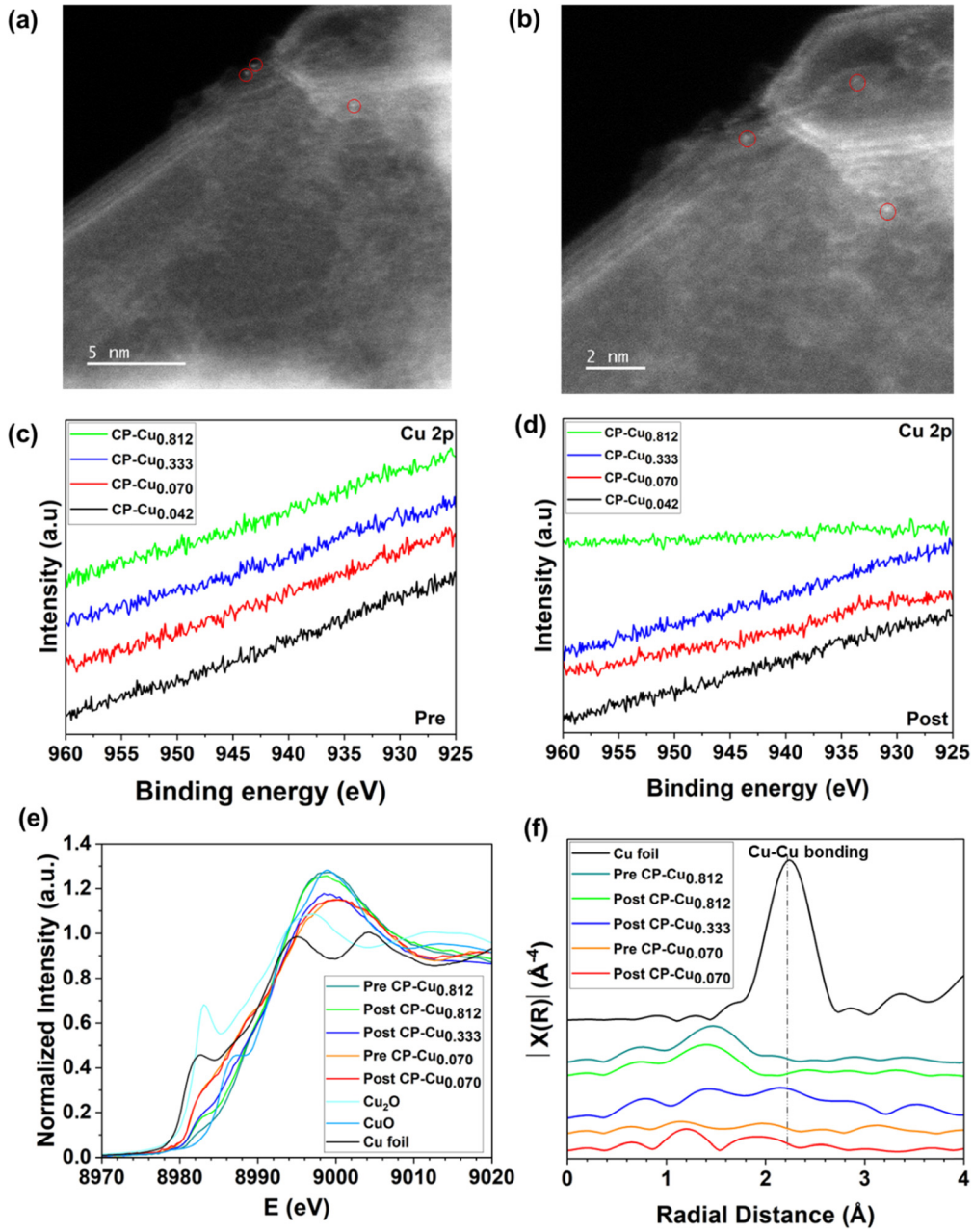

Fig. 4 Structural characterization of the CP–Cu electrodes. (a and b) AC-HAADF-STEM images of single atom Cu in the CP–$Cu_{0.812}$ post-electrode after the CORR. (c) High-resolution XPS spectra of Cu 2p of the pre-experiment CP–Cu electrodes. (d) High-resolution XPS spectra of Cu 2p of the post-experiment CP–Cu electrodes in the CORR. (e) Cu K-edge normalized XANES spectra as a function of incident photon energy (E) for the CP–Cu electrodes. (f) Fourier transform of k^3-weighted EXAFS in R space of the CP–Cu electrodes.

possible reason is that the CO_2 is more inert than CO, and the adoption of CO_2 on the Cu species is much more difficult than for CO.

Conclusions

We revealed the activity and selectivity of trace amounts of Cu with various loadings towards the CO/CO_2RR by simply impregnating Cu onto CP. An extraordinary mass specific activity and selectivity toward the CORR is observed with 50% FE of carbon products including the predominant CH_4 when the Cu loading is higher than 0.042 μg cm^{-2}. The predominant product switches from CH_4 to C_2 with an increase of Cu to 0.333 μg cm^{-2}. When further increasing the Cu loading to 0.812 μg cm^{-2}, the overall highest FE of C_2 achieves 78%, of which the major product of CH_3COO^- accounts for 42%. The record mass activities for CH_4 and C_2 reach 2435 and 584 A mg^{-1} of Cu, corresponding to TOFs of 267 and 145 s^{-1}, respectively. Different from the CORR, a higher loading of Cu is required to trigger the CO_2RR. Moreover, trace

Cu primarily catalyzes the CO_2RR to form C_1 (*e.g.*, CO and CH_4) even when the Cu loading reaches 0.812 μg cm^{-2}, indicating trace Cu is not in favor of C–C coupling in the CO_2RR. The effect of trace metal impurities can be extended to others that are active towards the CO_2RR, such as Zn for CO_2-to-CO conversion. We suggest that the effect of trace metal impurities must be quantified when developing metal-free and M–N–C catalysts for the CO/CO_2RR.

Disclaimer

This manuscript has been co-authored by UT-Battelle, LLC, under contract DE-AC05-00OR22725 with the US Department of Energy (DOE). The US government retains and the publisher, by accepting the article for publication, acknowledges that the US government retains a nonexclusive, paid-up, irrevocable, worldwide license to publish or reproduce the published form of this manuscript, or allow others to do so, for US government purposes. The DOE will provide public access to these results of federally sponsored research in accordance with the DOE Public Access Plan (**https://energy.gov/downloads/doe-public-access-plan**).

Conflicts of interest

There are no conflicts to declare.

Acknowledgements

This work is supported by the Office of Fossil Energy and Carbon Management of the U.S. Department of Energy under Award Number DE-FE0031919. A portion of this work was funded by ORNL's Laboratory Directed Research and Development (LDRD) Seed Money program. This research used resources of the Advanced Photon Source, an Office of Science User Facility operated for the U.S. Department of Energy (DOE) Office of Science by Argonne National Laboratory, and is supported by the U.S. DOE under Contract No. DE-AC02-06CH11357, and the Canadian Light Source and its funding partners.

References

1 J. Gu, S. Liu, W. Ni, W. Ren, S. Haussener and X. Hu, *Nat. Catal.*, 2022, **5**, 268–276.
2 Z. Han, D. Han, Z. Chen, J. Gao, G. Jiang, X. Wang, S. Lyu, Y. Guo, C. Geng and L. Yin, *Nat. Commun.*, 2022, **13**, 1–10.
3 J. Timoshenko, A. Bergmann, C. Rettenmaier, A. Herzog, R. M. Arán-Ais, H. S. Jeon, F. T. Haase, U. Hejral, P. Grosse and S. Kühl, *Nat. Catal.*, 2022, **5**, 259–267.
4 T. Zhang, J. C. Bui, Z. Li, A. T. Bell, A. Z. Weber and J. Wu, *Nat. Catal.*, 2022, **5**, 202–211.
5 F. P. García de Arquer, C.-T. Dinh, A. Ozden, J. Wicks, C. McCallum, A. R. Kirmani, D.-H. Nam, C. Gabardo, A. Seifitokaldani and X. Wang, *Science*, 2020, **367**, 661–666.
6 Z. Li, Y. Fang, J. Zhang, T. Zhang, J. D. Jimenez, S. D. Senanayake, V. Shanov, S. Yang and J. Wu, *J. Mater. Chem. A*, 2021, **9**, 19932–19939.
7 F. Li, A. Thevenon, A. Rosas-Hernández, Z. Wang, Y. Li, C. M. Gabardo, A. Ozden, C. T. Dinh, J. Li and Y. Wang, *Nature*, 2020, **577**, 509–513.
8 P. Saha, S. Amanullah and A. Dey, *Acc. Chem. Res.*, 2022, 11214–11217.
9 W. Choi, S. Park, W. Jung, D. H. Won, J. Na and Y. J. Hwang, *ACS Energy Lett.*, 2022, **7**, 939–945.
10 D. Wakerley, S. Lamaison, J. Wicks, A. Clemens, J. Feaster, D. Corral, S. A. Jaffer, A. Sarkar, M. Fontecave and E. B. Duoss, *Nat. Energy*, 2022, 1–14.
11 Y. Li, A. Ozden, W. R. Leow, P. Ou, J. E. Huang, Y. Wang, K. Bertens, Y. Xu, Y. Liu and C. Roy, *Nat. Catal.*, 2022, **5**, 185–192.
12 J. L. Hitt, Y. G. C. Li, S. S. Tao, Z. F. Yan, Y. Gao, S. J. L. Billinge and T. E. Mallouk, *Nat. Commun.*, 2021, **12**, 1114.
13 A. K. Ummireddi, S. K. Sharma and R. G. S. Pala, *J. Catal.*, 2022, 213–221.
14 C. Li, H. Xiong, M. He, B. Xu and Q. Lu, *ACS Catal.*, 2021, **11**, 12029–12037.
15 T. Zhang, X. Li, Y. Qiu, P. Su, W. Xu, H. Zhong and H. Zhang, *J. Catal.*, 2018, **357**, 154–162.
16 Z. Wu, H. Wu, W. Cai, Z. Wen, B. Jia, L. Wang, W. Jin and T. Ma, *Angew. Chem.*, 2021, **133**, 12662–12667.
17 F. Cheng, X. Zhang, K. Mu, X. Ma, M. Jiao, Z. Wang, P. Limpachanangkul, B. Chalermsinsuwan, Y. Gao and Y. Li, *Energy Technol.*, 2021, **9**, 2000799.
18 J. Li, J. Li, X. Liu, J. Chen, P. Tian, S. Dai, M. Zhu and Y.-F. Han, *Appl. Catal., B*, 2021, **298**, 120581.
19 R. O. Yang, J. Y. Duan, P. P. Dong, Q. L. Wen, M. Wu, Y. W. Liu, Y. Liu, H. Q. Li and T. Y. Zhai, *Angew. Chem., Int. Ed.*, 2022, **21**, DOI: **10.1002/anie.202116706**.
20 G. D. Shi, Y. L. Xie, L. L. Du, X. L. Fu, X. J. Chen, W. J. Xie, T. B. Lu, M. J. Yuan and M. Wang, *Angew. Chem., Int. Ed.*, 2022, **61**, DOI: **10.1002/anie.202203569**.
21 Y. B. Ma, J. L. Yu, M. Z. Sun, B. Chen, X. C. Zhou, C. L. Ye, Z. Q. Guan, W. H. Guo, G. Wang, S. Y. Lu, D. S. Xia, Y. H. Wang, Z. He, L. Zheng, Q. B. Yun, L. Q. Wang, J. W. Zhou, P. Y. Lu, J. W. Yin, Y. F. Zhao, Z. B. Luo, L. Zhai, L. W. Liao, Z. L. Zhu, R. Q. Ye, Y. Chen, Y. Lu, S. B. Xi, B. L. Huang, C. S. Lee and Z. X. Fan, *Adv. Mater.*, 2022, **34**, 2110607.
22 Y. Y. Liu, H. L. Zhu, Z. H. Zhao, N. Y. Huang, P. Q. Liao and X. M. Chen, *ACS Catal.*, 2022, **12**, 2749–2755.
23 T. Y. Zhang, J. C. Bui, Z. Y. Li, A. T. Bell, A. Z. Weber and J. J. Wu, *Nat. Catal.*, 2022, **5**, 202–211.
24 X. Chang, A. Malkani, X. Yang and B. Xu, *J. Am. Chem. Soc.*, 2020, **142**, 2975–2983.
25 W. Ma, X. He, W. Wang, S. Xie, Q. Zhang and Y. Wang, *Chem. Soc. Rev.*, 2021, **50**, 12897–12914.
26 Y. Lum, Y. Kwon, P. Lobaccaro, L. Chen, E. L. Clark, A. T. Bell and J. W. Ager, *ACS Catal.*, 2016, **6**, 202–209.
27 X. Fu, Y. Wang, H. Shen, Y. Yu, F. Xu, G. Zhou, W. Xie, R. Qin, C. Dun and C.-W. Pao, *Mater. Today Phys.*, 2021, **19**, 100418.
28 W. Rong, H. Zou, W. Zang, S. Xi, S. Wei, B. Long, J. Hu, Y. Ji and L. Duan, *Angew. Chem., Int. Ed.*, 2021, **60**, 466–472.

29 H. Yang, Y. Wu, Q. Lin, L. Fan, X. Chai, Q. Zhang, J. Liu, C. He and Z. Lin, *Angew. Chem.*, 2018, **130**, 15702–15706.
30 J. Zhao, Z. Chen and J. Zhao, *J. Mater. Chem. A*, 2019, **7**, 4026–4035.
31 J. Li, W.-Y. Zan, H. Kang, Z. Dong, X. Zhang, Y. Lin, Y.-W. Mu, F. Zhang, X.-M. Zhang and J. Gu, *Appl. Catal., B*, 2021, **298**, 120510.
32 T. Zhang, W. Li, K. Huang, H. Guo, Z. Li, Y. Fang, R. M. Yadav, V. Shanov, P. M. Ajayan and L. Wang, *Nat. Commun.*, 2021, **12**, 1–9.
33 R. M. Yadav, Z. Li, T. Zhang, O. Sahin, S. Roy, G. Gao, H. Guo, R. Vajtai, L. Wang and P. M. Ajayan, *Adv. Mater.*, 2022, **34**, 2105690.
34 L. Han, S. Song, M. Liu, S. Yao, Z. Liang, H. Cheng, Z. Ren, W. Liu, R. Lin, G. Qi, X. Liu, Q. Wu, J. Luo and H. L. Xin, *J. Am. Chem. Soc.*, 2020, **142**, 12563–12567.
35 J. Wu, S. Ma, J. Sun, J. I. Gold, C. Tiwary, B. Kim, L. Zhu, N. Chopra, I. N. Odeh and R. Vajtai, *Nat. Commun.*, 2016, **7**, 1–6.
36 Y. M. Liu, S. Chen, X. Quan and H. T. Yu, *J. Am. Chem. Soc.*, 2015, **137**, 11631–11636.
37 Y. M. Liu, Y. J. Zhang, K. Cheng, X. Quan, X. F. Fan, Y. Su, S. Chen, H. M. Zhao, Y. B. Zhang, H. T. Yu and M. R. Hoffmann, *Angew. Chem., Int. Ed.*, 2017, **56**, 15607–15611.
38 C. H. A. Wong, Z. Sofer, M. Kubešová, J. Kučera, S. Matějková and M. Pumera, *Proc. Natl. Acad. Sci. U. S. A.*, 2014, **111**, 13774–13779.
39 G. Dong, M. Fang, H. Wang, S. Yip, H.-Y. Cheung, F. Wang, C.-Y. Wong, S. T. Chu and J. C. Ho, *J. Mater. Chem. A*, 2015, **3**, 13080–13086.
40 A. Wuttig and Y. Surendranath, *ACS Catal.*, 2015, **5**, 4479–4484.
41 M. Li, H. Wang, W. Luo, P. C. Sherrell, J. Chen and J. Yang, *Adv. Mater.*, 2020, **32**, 2001848.
42 A. S. Varela, W. Ju, A. Bagger, P. Franco, J. Rossmeisl and P. Strasser, *ACS Catal.*, 2019, **9**, 7270–7284.
43 A. S. Varela, W. Ju and P. Strasser, *Adv. Energy Mater.*, 2018, **8**, 1703614.
44 P. Zhu, C. Xia, C.-Y. Liu, K. Jiang, G. Gao, X. Zhang, Y. Xia, Y. Lei, H. N. Alshareef and T. P. Senftle, *Proc. Natl. Acad. Sci. U. S. A.*, 2021, **118**, 2010868118.
45 W. Luc, X. Fu, J. Shi, J.-J. Lv, M. Jouny, B. H. Ko, Y. Xu, Q. Tu, X. Hu, J. Wu, Q. Yue, Y. Liu, F. Jiao and Y. Kang, *Nat. Catal.*, 2019, **2**, 423–430.
46 L. L. Zhuo, P. Chen, K. Zheng, X. W. Zhang, J. X. Wu, D. Y. Lin, S. Y. Liu, Z. S. Wang, J. Y. Liu and D. D. Zhou, *Angew. Chem.*, 2022, **134**, e202204967.
47 S. Y. Lee, H. Jung, N.-K. Kim, H.-S. Oh, B. K. Min and Y. J. Hwang, *J. Am. Chem. Soc.*, 2018, **140**, 8681–8689.
48 A. Eilert, F. S. Roberts, D. Friebel and A. Nilsson, *J. Phys. Chem. Lett.*, 2016, **7**, 1466–1470.
49 F. Huang, Y. Deng, Y. Chen, X. Cai, M. Peng, Z. Jia, J. Xie, D. Xiao, X. Wen and N. Wang, *Nat. Commun.*, 2019, **10**, 1–7.
50 H. Xu, D. Rebollar, H. He, L. Chong, Y. Liu, C. Liu, C.-J. Sun, T. Li, J. V. Muntean and R. E. Winans, *Nat. Energy*, 2020, **5**, 623–632.